Sains Malaysiana 52(11)(2023): 3307-3323
http://doi.org/10.17576/jsm-2023-5211-21

Carbon Quantum Dots Coupled Au Nanoparticle as Fluorescence-Based DNA Biosensors For Dengue Virus Detection

(Titik Kuantum Karbon Digandingkan Au Nanozarah Berasaskan Pendarfluor Biosensor DNA untuk Pengesanan Virus Denggi)

YAKUBU NEWMAN MONDAY[1,4], JAAFAR ABDULLAH[1,2,*], NOR AZAH YUSOF[1,2], SURAYA ABDUL RASHID[2], RAFIDAH HANIM SHUEB[3] & HAMIDAH SIDEK[5]

[1]Department of Chemistry, Faculty of Science, Universiti Putra Malaysia, 43400 UPM Serdang, Selangor, Malaysia
[2]Institute of Nanoscience and Nanotechnology, Universiti Putra Malaysia, 43400 UPM Serdang, Selangor, Malaysia
[3]Department of Medical Microbiology & Parasitology, School of Medical Sciences, Universiti Sains Malaysia, 16150 Kubang Kerian, Kelantan, Malaysia
[4]Department of Chemistry, Faculty of Science, Federal University Lokoja, P.M.B 1154, Lokoja, Kogi State, Nigeria
[5]Industrial Centre of Innovation in Sensor, SIRIM Berhad, No.1, Persiaran Dato' Menteri, Section 2, P.O. Box 7035, 40700 Shah Alam, Selangor, Malaysia

Received: 9 August 2023/Accepted: 1 December 2023

ABSTRACT

This study introduces a novel DNA biosensor probe comprising carbon quantum dots (CQDs) derived from palm kernel shell biomass and gold nanoparticles (AuNPs) synthesized via the citrate reduction method. The CQDs were doped with ethylenediamine using a hydrothermal process employing a one-pot synthesis method in an autoclave batch reactor. The resulting CQDs exhibited exceptional photoluminescent (PL) properties, with an excitation wavelength of 360 nm and an emission wavelength of 430 nm. Transmission electron microscope (TEM) images showed the average particle sizes of the CQDs and AuNPs to be 2 nm and 15 nm, respectively. Carboxylic acid-modified CQDs were coupled to amine-modified ssDNA (P_A) to construct the biosensor through the amine coupling technique. The AuNPs were modified through thiol coupling with Rhodamine B, L-cysteine, and thiol-modified ssDNA (P_T). Both P_A and P_T probes were designed to complement the DEN-3 virus oligonucleotide. CQDs acted as fluorophores and energy donors in the biosensor, while the AuNPs functioned as nanoquenchers of fluorophores and energy acceptors. The resulting probe pair, CQDs-P_A, and AuNPs-P_T demonstrated remarkable Förster resonance energy transfer (FRET) and exhibited fluorescence turn-on upon titration with DEN-3. The biosensor displayed excellent sensitivity with a logarithmic calibration equation of $5.22\text{Log}C + 20.79$ ($R^2 = 0.979$), covering a linear range of 0.001 nM to 100 nM. The limit of detection (LOD) was determined to be 1.57 ± 0.71 nM. This innovative DNA biosensor, incorporating CQDs and AuNPs, holds promising potential for sensitive and specific detection of the DEN-3 virus.

Keywords: Carbon quantum dots; dopants; FRET; palm kernel shell; quantum yield

ABSTRAK

Kajian ini memperkenalkan prob biosensor DNA baharu yang terdiri daripada titik kuantum karbon (CQD) yang diperoleh daripada biojisim tempurung isirong sawit dan nanozarah emas (AuNPs) yang disintesis melalui kaedah penurunan sitrat. CQD telah didop dengan etilenadiamina menggunakan proses hidroterma kaedah sintesis satu periuk dalam reaktor kelompok autoklaf. CQD yang terhasil menunjukkan sifat fotoluminesen (PL) yang luar biasa, dengan panjang gelombang pengujaan 360 nm dan panjang gelombang pancaran 430 nm. Imej mikroskop elektron penghantaran (TEM) menunjukkan purata saiz zarah CQD dan AuNP masing-masing adalah 2 nm dan 15 nm. CQD yang diubah suai asid karboksilik digabungkan dengan ssDNA (P_A) yang diubah suai amina untuk membina biosensor melalui teknik gandingan amina. AuNPs telah diubah suai melalui gandingan tiol dengan Rodamina B, L-cisteina dan ssDNA (P_T) yang diubah suai tiol. Kedua-dua prob P_A dan P_T direka untuk melengkapkan oligonukleotida virus

DEN-3. CQD bertindak sebagai fluorofor dan penderma tenaga dalam biosensor manakala AuNP berfungsi sebagai nano-pelindapkejut fluorofor dan penerima tenaga. Pasangan prob yang terhasil, CQDs-P_A dan AuNPs-P_T menunjukkan pemindahan tenaga resonans Förster (FRET) yang luar biasa dan menunjukkan pendarfluor hidup semasa pentitratan dengan DEN-3. Biosensor memaparkan kepekaan yang sangat baik dengan persamaan penentukuran logaritma 5.22LogC + 20.79 (R^2 = 0.979), meliputi julat linear 0.001 nM hingga 100 nM. Had pengesanan (LOD) ditentukan sebagai 1.57 ± 0.71 nM. Biosensor DNA yang inovatif ini menggabungkan CQD dan AuNP, berpotensi untuk pengesanan sensitif dan khusus virus DEN-3.

Kata kunci: Dopan; FRET; hasil kuantum; tempurung isirong sawit; titik kuantum karbon

Introduction

Dengue fever, caused by the dengue (DEN) virus, is a significant global public health concern affecting people worldwide. DEN virus belongs to a family of pathogenic viruses called Flaviviridae, which includes other viruses like the West Nile virus, Japanese encephalitis virus, yellow fever virus, and Zika virus. The primary mode of transmission for DEN virus is through female *Aedes aegypti* and *Aedes albopictus* mosquitoes, which spread the virus from person to person. DEN virus is classified within the Flavivirus genus and is divided into four distinct serotypes: DEN-1, DEN-2, DEN-3, and DEN-4 viruses (Jahwarhar Izuan & Nor Azah 2018; Sheh Omar et al. 2020; Wasik, Mulchandani & Yates 2018). These serotypes have a single-stranded RNA genome and can cause dengue fever (DF), a mild febrile illness, during primary infection. However, in some cases, the virus can lead to more severe conditions such as dengue hemorrhagic fever (DHF) and dengue shock syndrome (DSS), as categorized by the World Health Organization (WHO) (Darwish, Yatimah & Khor 2015; Rashid et al. 2015).

Approximately 2.5-3.6 billion people, nearly 50% of the global population, are at risk of DEN virus infection. Each year, there are an estimated 50-100 million cases of dengue fever, resulting in 22,000-24,000 deaths and 500,000 cases of DHF (Jahwarhar Izuan & Nor Azah 2018). Unfortunately, there are currently no effective vaccines available for dengue. The management of the disease primarily involves fluid replacement therapy and the use of Dengvaxia (CYD-TDV). This controversial vaccine has recently been licensed and approved by the World Health Organization (WHO) and the US Food and Drug Administration (FDA) for DEN virus (Jahwarhar Izuan & Nor Azah 2018; WHO 2018). Common symptoms of dengue fever include fever, headache, rashes, severe joint pain, and muscle and motor neuron system disorders. If not detected, diagnosed, and treated early, these symptoms can progress to severe dengue, which can be life-threatening. Unfortunately, dengue symptoms can often be mistaken for other illnesses such as influenza, measles, malaria, typhus, yellow fever, and other viral infections (Samsulida et al. 2014).

Therefore, the early detection of dengue is crucial to the accurate diagnosis and treatment of the disease and effectively differentiate it from other similar febrile illnesses. Typically, the diagnosis of DEN virus is carried out three to five days after the onset of symptoms using serological tests or conventional detection methods (Gosink 2014). Mosquitoes transmit DEN virus and elicit an immune response in the body, producing antibodies against the DEN virus (E) protein (antigens). The described phenomenon forms the basis of antibody-based biosensors, also known as immunosensors. However, immunosensors rely on specific interactions between antibodies and antigens (Sentürk et al. 2018), which limits their effectiveness due to the delayed production of antibodies after 3-5 days of infection.

Consequently, early detection using this method is highly unlikely. Hence, to overcome this limitation, alternative approaches have been proposed, such as detecting the pathogen or antigens such as the non-structural 1 (NS1) protein, ribonucleic acid (RNA), or complementary deoxyribonucleic acid (cDNA) that complements a single-stranded DNA (ssDNA) probe (Samsulida et al. 2014; Sheh Omar et al. 2018). Diagnostic serological methods for detecting DENV infection include enzyme-linked immunosorbent assay (ELISA) or lateral flow for detecting the viral NS1 protein, polymerase chain reaction (PCR), immunofluorescence assay (IFA), reverse transcribed polymerase chain reaction (RT-PCR), and real-time polymerase chain reaction (real-time PCR). However, these methods can be laborious, requiring sophisticated and expensive equipment and highly trained personnel (Plennevaux et al. 2016; Rashid et al. 2015). Researchers have reported low relative sensitivity, specificity, selectivity,

and turnaround time for some of these methods, with a high incidence of false-negative or false-positive results. Consequently, scientists have been racing to enhance, improve, and discover new DEN virus detection and diagnostic techniques that offer reasonable sensitivity, specificity, selectivity, shorter turnaround time, lower cost, and require less specialized training (E. Alahi & Mukhopadhyay 2017). Consequently, extensive research has been conducted on applying biosensors in various forms to analytes and pathogen detection (Xiao et al. 2023; Yan et al. 2022).

This research focuses on the development of a DNA biosensor probe, which consists of carboxylic acid-modified carbon quantum dots (CQDs) derived from palm kernel shell biomass, as well as citrate-capped gold nanoparticles (AuNPs) synthesized in an aqueous solution. The carboxylic acid-modified CQDs serve as fluorophores and energy donors, while the AuNPs act as nanoquenchers and energy acceptors. Palm kernel shell biomass is a significant waste product from palm oil and palm product production, which is abundantly available in Malaysia. It mainly consists of cellulose, hemicellulose, and lignin, making it rich in carbon materials capable of producing CQDs of impressive optical properties.

By thermally reducing the palm kernel shell in an inert nitrogen environment, the mentioned components are converted into a black graphitic carbonaceous material rich in carbon, achieved by carbonization at a temperature of 400 ℃ for over 2 h. This carbonized palm kernel shell (CPKS) can then be utilized as a raw material for synthesizing CQDs using the amine-coupling technique. The CQDs so prepared were modified and conjugated with amine-modified ssDNA (9-mer) through a procedural sequence to complement the DEN-3 virus oligonucleotide. On the other hand, the AuNPs were modified with Rhodamine B, L-cysteine, and thiol-modified ssDNA (9-mer) to complete the DEN-3 virus oligonucleotide via the thiol-coupling process. It has been established by Tseng, Hu and Chiu (2019) that Rhodamine B is adsorbed to the surface of AuNPs through electrostatic interaction and such modification cause AuNPs dispersion stability and made them to be target specific (Draz & Shafiee 2018; Zhang 2013). The resulting biosensor was utilized as a fluorescence resonance energy transfer (FRET) probe to detect serotype-3 dengue virus DNA.

In the procedure, when the gold nanoconjugate is added to the modified CQDs, it diminishes the fluorescence intensity of the CQDs fluorophore because the gold nanoconjugate clusters around the fluorophore, reducing the fluorescence intensity of the CQDs nanoconjugates. Despite the clustering of Au-nanoconjugates near the CQDs fluorophore, the two nanoconjugates are positioned far apart to allow the FRET phenomenon because the two nanoconjugates carry ssDNA with similar sequences. Still, one is amine-modified, and the other is thiol-modified. As a result, they repel each other, preventing the formation of a duplex structure.

When complementary DNA (cDNA) is introduced, which has the correct sequence to form a duplex with both ssDNA on the nanoconjugates, it reacts with the DNA probe sequence on the nanoconjugates causing the nanoconjugate to approach the cDNA to form a duplex, bringing the CQDs and AuNPs closer. Consequently, energy transfer occurs from the fluorophore (CQDs) to the acceptor (AuNPs) (Figure 1). The fluorescence recovery exhibits a switch-on phenomenon, where the fluorescence intensity increases proportionally with the concentration of the cDNA (Nasrin et al. 2018; Sabzehparvar et al. 2019).

Figure 1 represents a schematic illustration of the three-step methodology for synthesizing, modifying, and detecting the DEN-3 virus. Step 1 demonstrates the synthesis and modification of CQDs for the first probe pairs, while Step 2 involves synthesizing and modifying AuNPs for the second probe pairs. Finally, Step 3 illustrates the reaction between the probe pairs and the cDNA, forming a duplex as a mechanistic FRET detection strategy for the DEN-3 virus.

Materials and Methods

Chemicals and Materials

The following chemicals and reagents used in this research were analytical grade. Ultra-pure water (Milli-Q), with a resistivity of 18.2 mΩ/cm from Thermo Scientific Barnstead smart2pure system (Fisher Scientific, UK). Ethylenediamine (EDA) (Acros Organics, USA), L-Cysteine (L-Cyst: Merck U.S.A), sodium hydroxide (NaOH: R & M Chemicals, UK), Hydrochloric acid (HCl: HmbG Chemicals), Phosphate Saline buffer, pH 7.4 (Bendosen, Malaysia), N-hydroxysuccinimide (NHS: Alfa Aesar England), 1-ethyl-3-(3-dimethyl-aminopropyl) carbodiimide (EDC: Great Britain), Sodium chloroacetate (Sigma- Aldrich, USA), tris(2-carboxyethyl) phosphine hydrochloride (TECEP: Sigma Aldrich, India), Absolute ethanol (EtOH: Fisher Scientific, UK), and hydrochloric acid (HCl: HmbG Chemicals,

Germany). Sulphuric acid (H2SO4: Fisher Scientific, UK), quinine sulfate (QS: Fisher Scientific, France), tri-sodium citrate (R & M Chemicals, UK), Chloroauric acid (HAuCl4: Sigma Aldrich USA), Mercaptopropionic acid (MPA: Sigma Aldrich, USA), L-cysteine (L-Cyst: Merck, Japan), Rhodamine B (RB: Sigma Aldrich, India), DNA sequences obtained from Apical Scientific Sdn. Bhd. (Malaysia) as contained in Table 1.

INSTRUMENTATION AND APPARATUS

The following instrument and apparatus were used in this research work. The tools include Protech Oven: Model FAC-50 Malaysia, Spark multimode microplate reader fluorometer, Infinites F500, TECAN, Ltd, Mannedorf, Switzerland, and Ultra-Violet Visible Spectrophotometer (Perkin Elmer Lambda 35 UV-Visible Spectrophotometer, USA). Fourier-transform Infra-red Spectrophotometry (FTIR), Transmission Electron Microscopy-coupled with Energy Dispersive X-ray (TEM-EDX), and Dynamic light scattering (DLS) measurement with a Zetasizer Nano ZS instrument (Malvern Instruments, Malvern, England), Munktell filter paper 110 mm with 3-5 µm pore size (Ahlstrom, Sweden), syringe filter, 25 mm and 0.22 µm pore size (CNW Technologies, China) and 3500 – 14000 Da Viskase Membra Cel MD 77 Dialysis membranes-USA, Amicon Ultra-4 centrifugal filter, Ultracel-30K, Merck millipore-Ireland (Adegoke & Park 2017; Saheeda et al. 2019).

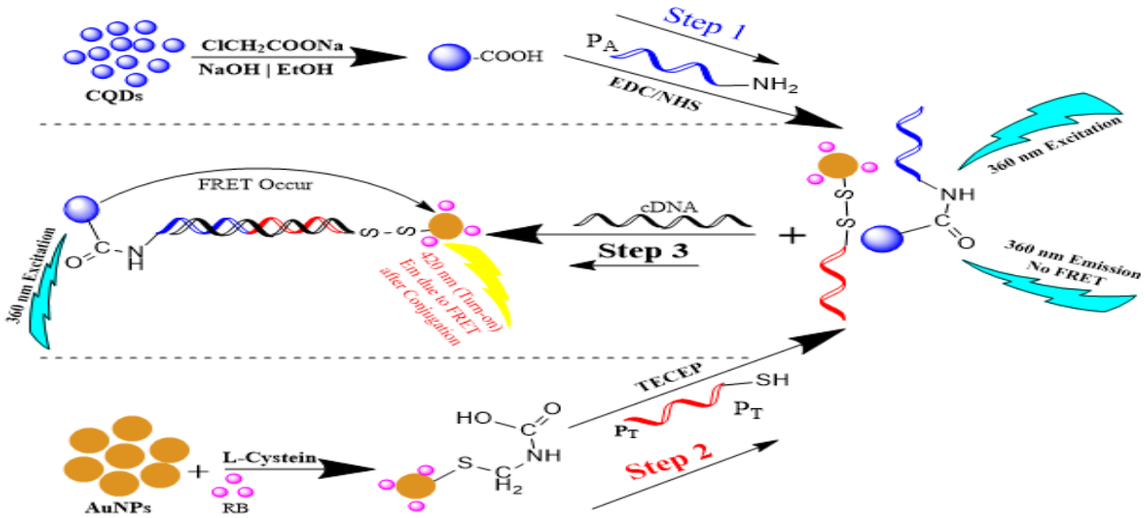

FIGURE 1. Schematics of the synthesis and modification of CQDs (Step 1), synthesis and transformation of AuNPs (Step 2), and interaction of the probe pairs with the cDNA to form a duplex (Step 3)

TABLE 1. The sequences of nucleotide probe (DNAs) used in this study

NAME	SEQUENCE
ssDEN-3 Probe = P_A = (ssDNA-3)NH_2	5'-TCA CTC TGG-$(NH_2)(CH_2)_6$-3'
ssDEN-3 Probe = P_T = SH(ssDNA-3)	5'-SH-$(CH_2)_6$-ACG AGA CCT-3'
ctDEN-3 Complementary Target Sequence ctDNA-3	5'-CCA GAG TGA AGG TCT CGT-3'
ncDEN-3 Non-Complementary Sequence ncDNA-3	5'-GGT CTC ACT TCC AGA GCA-3'
smDEN-3 Single Based Mismatch Sequence smDNA-3	5'-GGT CTC A**G**T TCC AGA GCA-3

HYDROTHERMAL SYNTHESIS OF NITROGEN-DOPED CARBON QUANTUM DOTS (CQDs-N)

Nitrogen-doped carbon quantum dots (N-CQDs) having an amino-functional group (CQDs-NH_2) were synthesized via hydrothermal synthesis from Carbonized palm kernel shell (CPKS) biomass. Briefly, 0.3 g of powdered CPKS was dissolved in 15 mL deionized water (dH_2O), 3 mL of 1 M NaOH and 1 mL ethylenediamine (EDA) were added and stirred for 30 min. Next, the mixture was transferred to an airtight Teflon-lined stainless-steel autoclave batch reactor for hydrothermal treatment at 160 ℃ for 3 h and then brought to 40 ℃ after the reaction. First, the mixture was filtered using filter paper, then a syringe filter was attached to a 20 mL syringe, and the pH was adjusted to 7.03 to obtain N-CQDs or CQDs-NH_2, Figure 2 (Bhattacharya, Mishra & De 2017; Yakubu et al. 2021).

CQDs SURFACE MODIFICATION WITH CARBOXYLIC ACID FUNCTIONAL GROUP

A mass of 0.3 g of sodium chloroacetate, NaOH, and 1 mL EtOH was dissolved in 200 mL of the as-synthesized CQDs and sonicated for 2 h. Then, the pH of the as-synthesized CQDs was adjusted to 6.5 by titrating against dilute hydrochloric acid (HCl). The solution was concentrated at 40 mL in an oven at 55 ℃ and was dialyzed in 200 mL dH_2O to obtain CQDs-COOH. Finally, CQDs-COOH were freeze-dried, and a stock solution of 124.4 mg/mL was obtained by dissolving the powdered CQDs in PBS (Sun et al. 2012; Suria et al. 2020).

CONJUGATION OF NH_2-ssDNA TO CQDs-COOH

Amine-modified ssDNA (NH_2-ssDNA: PA) was conjugated by amine coupling to the CQDs-COOH to obtain DNA biosensor probe pair PA1, according to the modified work of (Sabzehparvar et al. 2019; Suria et al. 2020). In adherence to EDC crosslinker protocol, 6 mL of aqueous 10 mg/mL CQDs-COOH in PBS, pH 7.0 solution was sonicated for 15 min, activated with 1 mL of freshly prepared 0.1 M solution of EDC, vortexed for 2 min, and sonicated for 1 h. Then, 800 µL of 0.1 M NHS and 120 µL of 100 µM amine-modified ssDNA were pipetted into the solution almost simultaneously and vortexed for 1 min to obtain a 1.52 µM DNA concentration. The mixed solution was left overnight (24 h). Finally, the solution was ultrafiltered using the centrifugal filter at 4000 rpm to purify it, obtain purified amine-modified probe PA1, and store it at 4 °C.

SYNTHESIS OF CITRATE-CAPPED AuNPs

A typical procedure for AuNP synthesis using the citrate reduction method was explored. Briefly, 1 mL of 50 mM HAuCl4 (393.83 g/mol) was added to 49 mL of Milli-Q water to concentrate one mM in a beaker. The solution was pale yellow in a beaker with a magnetic stirrer, and the beaker was placed on a hot plate heated at 105 °C in a fume hood. Next, 5 mL of colorless 38.8 mM tri-sodium citrate (294.10 g/mol) was added to the solution, and the pale-yellow coloration fainted with time, and the solution turned dark violet to wine or deep red. The AuNPs solution was further boiled for 15 min, brought to room temperature, and stored at 4 ℃ for further use (Gao et al. 2019; Hamd-Ghadareh & Salimi 2019; Sabzehparvar et al. 2019).

MODIFICATION OF GOLD NANOPARTICLES (AuNPs) WITH THIOL COMPOUNDS

The following reagents were used for the surface modification of the AuNPs: Mercaptopropionic acid (MPA), L-cysteine (cyst), and Rhodamine B (RB). In the modification approach, five different modifications were prepared, thus: (1) a solution of 100 µL of 3.5×10^{-6} M RB was added to 1 mL AuNPs, (2) 100 µL of 5×10^{-6} M MPA was added to 1 mL AuNPs, (3) 100 µL of 5×10^{-6} M of L-cyst was added to 1 mL AuNPs, (4) 100 µL of 3.5×10^{-6} M RB and 100 uL 5×10^{-6} M MPA were added to 1 mL AuNPs and (5) 100 µL of 3.5×10^{-6} M RB and 100 uL 5×10^{-6} M of L-Cyst was added to 1 mL AuNPs solution. All the modified AuNPs were kept at 4 °C overnight (18 h) and then purified by subjecting the samples to centrifugation at 12000 rpm for 5 min. The upper layer was discarded, and the particles under the centrifuge tube were washed and resuspended in PBS (10 mM, pH 7.0, 50 mM NaCl) to their original volume (Guerrini, Alvarez-Puebla & Pazos-Perez 2018).

CONJUGATION OF THIOL-MODIFIED ssDNA TO AuNPs

600 µL of 3.5×10^{-6} M RB was added to 6 mL AuNPs, vortexed for 2 min, and left for 1 h, and 600 µL 5×10^{-6} M L-Cysteine was also added. The solution vortexed for 30 s and was kept overnight and purified by subjecting the samples to centrifugation at 12000 rpm for 5 min. The upper layer was discarded, and the particles under the centrifuge tube were washed and resuspended in PBS (10 mM, pH 7.0, 50 mM NaCl) to their original volume. Then, 118 µL of 100 µM thiol-modified ssDNA was added, and 400 µL of 50×10^{-6} M TECEP was swirled.

The solution was kept overnight to obtain (ssDNA-S-S-AuNPs-RB) nanoconjugate as PT2 (1.53 µM) (Guerrini, Alvarez-Puebla & Pazos-Perez 2018).

DETECTION OF SYNTHETIC DEN-3 VIRUS SAMPLE WITH THE FABRICATED FRET PROBE

The best ratio or proportion of CQDs-PA and AuNPs-PT was determined to understand the quenching efficiency of AuNPs on the CQDs fluorophores. To determine the proportion that produces the best biosensor probe's FRET efficiency or the best fluorescence intensity, the ratio of the nanoconjugate such as 1.5:1, 1:1, 1:1.5, 1:2.3, 1:4, 1:9, and 1:19 were mixed, and 100 µL of PBS (10 mM, pH 7.0, 50 mM NaCl) added and allowed to incubate for 30 min (Sabzehparvar et al. 2019). The determination was done using a 96-well Coaster microplate in a Tecan Microplate reader fluorometer equipped with Sparkco and Megalin 2.2 software. The effect of the incubation time: 5, 30, 60, 90, 120, and 150 min, temperature: 30, 35, 40 °C, and Buffer pH: 6.0, 6.5, 7.0, 7.5, 8.0 were studied, respectively. The ncDNA, smDNA, and synthetic samples (cDNA) were tested against the designed probe for the selectivity study. All the determinations were done in triplicates (n = 3).

RESULTS AND DISCUSSION

CHARACTERIZATION OF CQDs AuNPs

In synthesizing Carbon Quantum Dots (CQDs), we employed a Teflon-lined autoclave batch reactor and a one-step synthesis procedure to produce high-quality CQDs with excellent photoluminescence properties. The CQDs exhibited blue fluorescence under UV light, as shown in Figure 2. Additionally, we utilized a hydrothermal synthesis method described earlier to fabricate blue CQDs. Our results demonstrated that subjecting CPKS, derived from oven-calcinated PKS biomass containing cellulose, hemicellulose, and lignin, to synthesis procedure described in the methodology resulted in pyrolysis, nucleation,

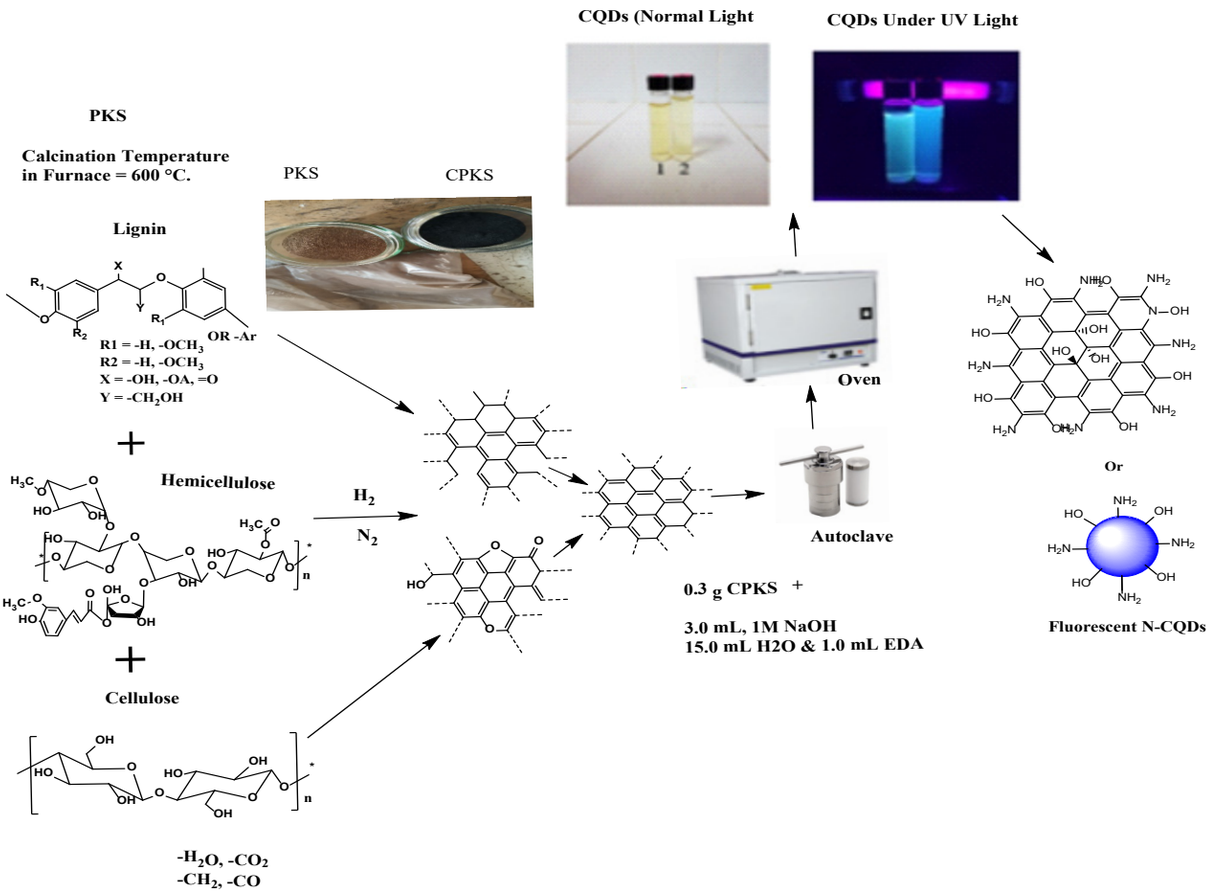

FIGURE 2. Processing of CPKS and synthesis of CQDs

condensation, polymerization, carbonization, and surface functionalization process, respectively. This process led to N-CQDs forming a conjugated system that enables the absorption of electromagnetic radiation and subsequent fluorescence emission (Hoan, Tam & Pham 2019; Pudza et al. 2019).

We introduced a carboxylic acid functional group using sodium chloroacetate to functionalize the CQDs' surface. The pH was adjusted to 6.5 using HCl and NaOH, and the resulting solution was dialyzed to obtain carboxylic acid-functionalized CQDs (CQDs-COOH) (Shylesh et al. 2010; Sun et al. 2012; Suria et al. 2020). The CQDs-COOH exhibited an optimal emission wavelength at 430 nm, with an excitation wavelength of 360 nm for our research application. To determine the appropriate concentration of CQDs-COOH with the desired emission peak, we prepared various concentrations of CQDs by dissolving the solid sample in PBS 7.4. Our results indicated that the fluorescence intensity increased as the nanomaterial concentration increased, from 0 to 15 mg/mL. Consequently, we selected a concentration of 10 mg/mL, which exhibited a fluorescence intensity of approximately 100,000 (a. u.), for further application.

The UV-Visible spectra of the CQDs and AuNPs were run to characterize them and their modified nanoconjugates. The UV-Visible spectra were obtained by scanning the materials within a wavelength range of 200-700 nm (Figure 3). The UV-Visible results of the N-CQDs (Figure 3a(i)) showed prominent absorption peaks at 260-280 nm and 320-340 nm. The 260-280 nm peak corresponds to the π-π* transition of aromatic C=C bonds in the core sp^2 hybridized carbon fragments and the conjugated π nanodomain within the CQDs

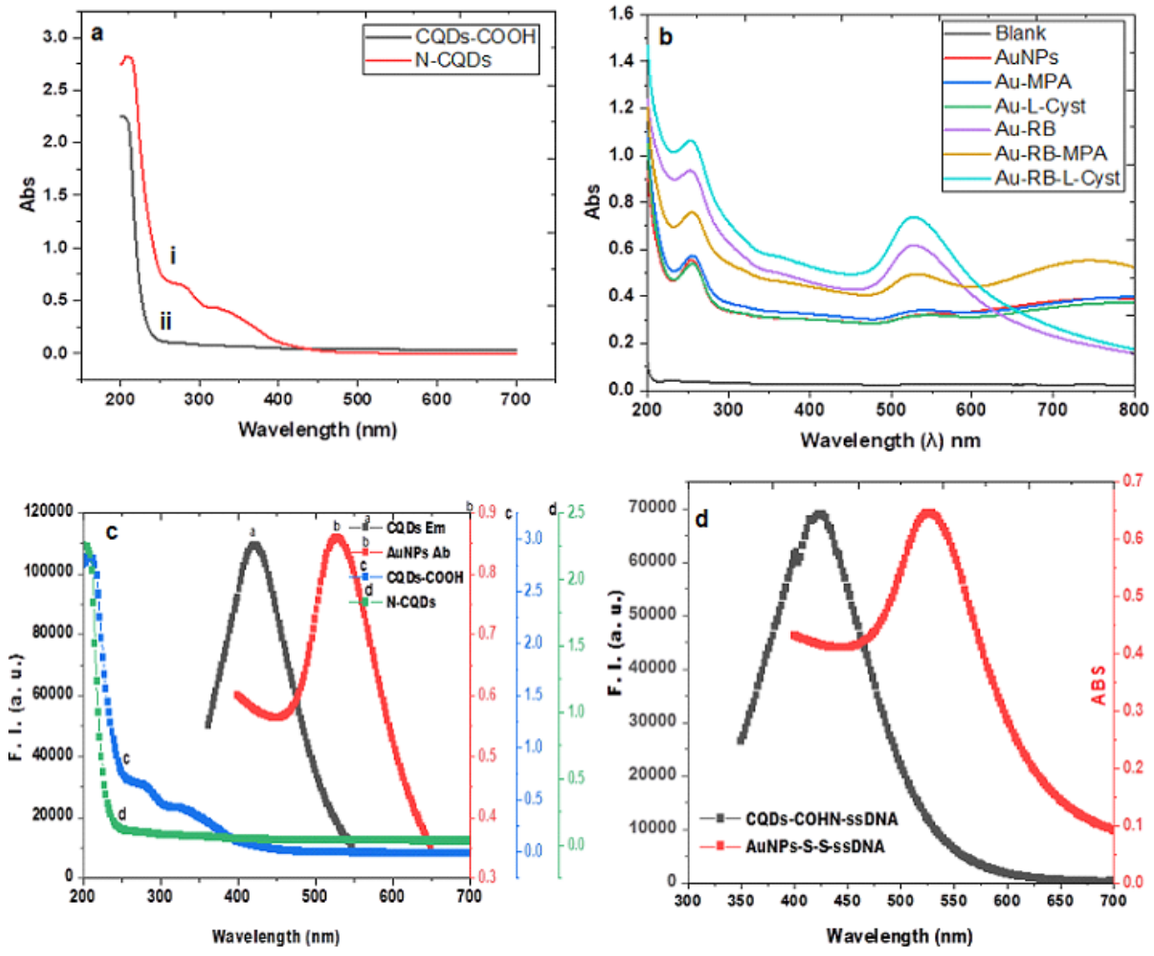

FIGURE 3. UV-Visible spectra of (a) i) CQDs-N (a) ii) CQDs-COOH (b) AuNPs and various modifications with MPA, L-Cysteine, RB, and a combination of RB-MPA and RB-L-Cysteine (c) emission and absorption spectra and spectra overlap of CQDs and AuNPs (d) emission and absorption spectra and spectra overlap of CQDs nanoconjugate and AuNPs nanoconjugate showing peaks reduction after conjugation

structure. The peak at 320-340 nm is attributed to the n-π* transition of non-bonding electrons in C=C and C=O, characteristic features of CQDs (Bajpai, D'Souza & Suhail 2019; Pudza et al. 2019; Stefanakis et al. 2014). However, these transition peaks were reduced as a result of the modification of the CQDs with the carboxylic acid functional group (-COOH) (Figure 3a(ii)), similar to the preliminary analysis in this work where the fluorescence intensity of CQDs-COOH at a concentration of 10 mg/mL is approximately 100,000 (a. u.). Still, when the CQDs are modified and conjugated with the probe (PA), the intensity drops to around 70,000 (a. u.).

In the typical fashion of AuNPs, Figure 3(b) presents the UV-Visible spectra of both unmodified AuNPs and AuNPs that underwent modifications using different reagents. These modifications resulted in varied absorption at 530 nm, indicated by different optical density (OD) values. Specifically, 100 µL of 5×10^{-6} M MPA, 5×10^{-6} M L-cysteine, and 3.5×10^{-6} M RB were utilized, followed by the addition of 100 µL each of RB-MPA and RB-L-cysteine to 1 mL of AuNPs. The mixture was then incubated at 4 °C in a refrigerator overnight.

The UV-Visible analysis showed that unmodified AuNPs exhibited the highest absorbance or OD value at 530 nm. Upon modification, a slight decrease in absorbance was observed in the following order: unmodified AuNPs > AuNPs-RB-L-Cysteine > AuNPs-RB > AuNPs-RB-MPA > AuNPs-MPA > AuNPs-L-Cysteine. This change in OD values can be attributed to the bonding between the AuNPs and the modification reagents. Consequently, altering the surface chemistry of the AuNPs modifies their optical properties, which, in turn, impacts various aspects of plasmon enhancement or quenching, excitation rate due to the local field effect, and emission rate through surface plasmon coupled emission during detection. These factors are pivotal in controlling fluorescence intensity (Chowdhury et al. 2020).

Considering the factors mentioned, the AuNPs-RB-L-Cysteine, which displayed the second-highest OD after unmodified AuNPs, was selected for further applications due to its properties closely resembling those of the unmodified AuNPs. Moreover, the difference in peaks between unmodified AuNPs and the modified form indicates successful conjugation of the modification reagents (RB and L-Cysteine) to the surface of the AuNPs, resulting in reduced OD (Guerrini, Alvarez-Puebla & Pazos-Perez 2018).

In Figure 3(c), we observed the alignment of the emission peak of CQDs when excited at a wavelength of 360 nm with the absorption peak of AuNPs. This result is presented in Figure 3(a) within the frame. The outcome shows that the emission peak of the CQDs and the absorption peak of AuNPs coincide with the maximum emission peak of the CQDs at 425 nm. In contrast, the maximum absorption peak of AuNPs is registered at 530 nm.

This alignment holds significance as the effectiveness of FRET relies on the spectral overlap between the emitted light of the donor molecules (CQDs) acting as fluorophores and the acceptor molecules (AuNPs) acting as nano-quenchers, as well as the distance between the two nanoparticles or nanoconjugates (Suria et al. 2020). Therefore, these two nanoconjugates form a suitable donor-acceptor pair capable of FRET if the spectral overlaps indicate they are close for FRET to occur (Chowdhury et al. 2020; Suria et al. 2020).

Figure 3(c) and 3(d) demonstrates the spectral overlap between the CQD-PA (CQDs-CONHssDNA) and AuNPs-PT (AuNPs-S-S-DNA) nanoconjugates, confirming their capability for FRET. The overlap does not significantly differ from the modified CQDs and AuNPs due to the proximity between the nanoconjugates, even after conjugation to DNAs, a phenomenon attributed to the short length of the DNA strands (9-mer). However, the disparity in intensities between the peaks of the nanoconjugates (Figure 3(c) and 3(d)) indicates that the modified nanoparticles, when DNA-conjugated, exhibit lower peak intensities in Figure 3(d) compared to those in Figure 3(c) (Sabzehparvar et al. 2019).

Vibrational spectroscopy studies and data are accessed through FTIR and Raman analysis to understand the chemical environment of CQDs. Still, we relied on FTIR to determine the functional group on the synthesized CQDs (Ma et al. 2019). In Figure 4(a), we observe the FTIR spectra of carbon quantum dots functionalized with ethylenediamine (CQDs-EDA (I)) alongside the spectra of ethylenediamine (EDA (II)). These spectra provide valuable insights into the structural chemical bonds and functional groups present in the CQDs (Suria et al. 2020). We can identify absorption bands in the CQD-EDA (I) and EDA (II) spectra. Notably, the EDA spectra exhibit 3357.4 cm^{-1} and 3288.0 cm^{-1} peaks corresponding to the stretching vibration of O-H and N-H bonds in primary aliphatic alcohols and amines (Segal & Eggerton 1961; Wang et al. 2015). Medium or small and broad absorption bands ranging from 3500 to 3200 cm^{-1} in the FTIR spectra are typically associated with N-H aliphatic amines (Dong et al. 2015). Furthermore, we can observe a functional group in the 1650-1590 cm^{-1}

range for all bands, indicating the scissoring vibration of a primary amine (-NH_2). This amino-functional group is present in both EDA and CQDs-EDA, confirming the presence of amine functionalization on the surface of the CQDs.

The CQDs exhibit similar broad and intense peaks at 3280.4 cm^{-1} (CQDs-EDA), suggesting the presence of a normal polymeric hydroxyl (O-H) group. Additionally, we can identify other mountains in the fingerprint region, specifically at 1360.0 cm^{-1}, 1405.9 cm^{-1}, 1085.7 cm^{-1}, 1041.4 cm^{-1}, and 879.4 cm^{-1}. These peaks likely correspond to the stretching vibrations and out-of-plane bending modes of sp^2 and sp^3 hybridized carbon-hydrogen (C-H) groups (Pudza et al. 2019; Yin et al. 2013).

In Figure 4(b) and 4(c), we present the transmission electron microscopy (TEM) images illustrating the morphological characteristics of the CQDs and AuNPs. The findings show that the synthesized nanoparticles are predominantly spherical and uniformly distributed. Furthermore, their particle sizes were determined to be 2.10 ± 0.06 nm for the CQDs and 16.00 ± 0.20 nm for the AuNPs. Notably, no visible clustering or significant aggregation among the particles was observed, indicating a monodisperse state within the aqueous solution (Suria et al. 2020; Sabzehparvar et al. 2019).

To determine the quantum yield (QY) of CQDs-EDA and CQDs-LPh, the photoluminescence properties of the CQDs were compared to those of quinine sulfate. Measurements were conducted using a UV-Visible spectrophotometer Lambda 35 for absorbance and a Tecan Multimode reader for fluorescence properties. The QY of CQDs-EDA was 13.5% at a concentration of 50.1 mg/mL, while CQDs-LPh exhibited a QY of 8.6% at 10.0 mg/mL.

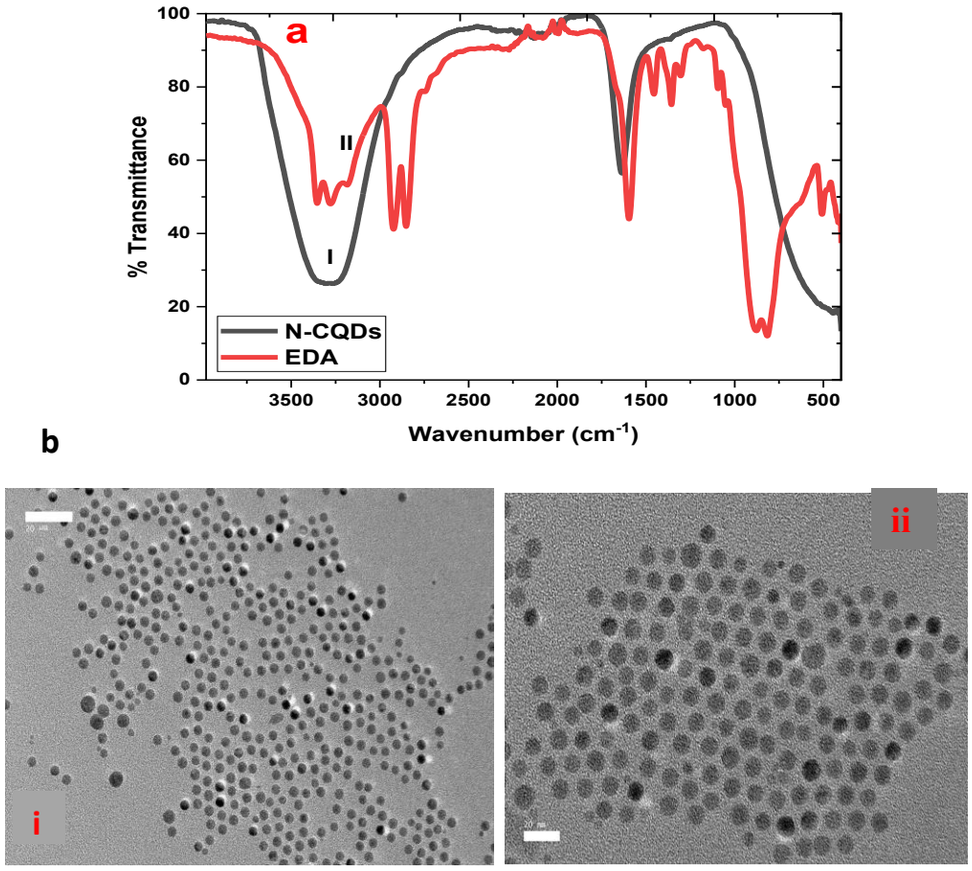

FIGURE 4. a) FTIR Spectra of CQDs (I) and EDA (II). b) TEM image of (**i**) CQDs and (**ii**) AuNPs

Comparing the QY of CQDs-EDA and CQDs-LPh to those of CQDs derived from other natural sources, it is evident that they have higher QY values. However, other CQDs have even higher QY values than those obtained in this study. Noteworthy examples of CQDs derived from other natural sources include Ginko fruit (3.33%) (Li et al. 2017), mangosteen pulp (1.09%) (Yang et al. 2017), prawn shell (9%) (Gedda et al. 2016), *Pyrus pyrifolia* or apple juice (4.27%) (Bhamore et al. 2018b), glucose (2.4%) (Yang et al. 2011), sugar cane bagasse (12.35%) (Du et al. 2014) banana juice (8.95%) (De & Karak 2013), microcrystalline cellulose (51%) (Wu et al. 2017), and *Acacia concinna* seed (10.2%) (Bhamore et al. 2018a).

Quantum yield measures the photoluminescence intensity of CQDs compared to a standard (Hoan, Tam & Pham 2019). It acts as a figure of merit for the optical performance of a fluorophore (Laverdant et al. 2011), reflecting the brightness and photon strength of CQDs while considering factors like photobleaching and photostability in fluorescence applications (Wang & Qiu 2016). The QY values were calculated using the established method described in the relevant section of the Supplementary Information, resulting in 8.5% and 13.7% for the CQDs. These findings demonstrate that PKS biomass has the potential to yield high-quality CQDs with excellent QY values for optical imaging and various other applications.

To support the TEM analysis discussed earlier, a powdered X-ray diffractometer device (Shimadzu XRD-600 powder-diffractometer, Japan) was employed to analyze the CQDs using X-ray diffraction (XRD). The instrument utilized Cuk (A = 1.540562 nm) with a voltage of 30.0 kV and a current of 30 mA. XRD, a fundamental analytical technique, played a crucial role in determining and identifying the structure, purity, and crystallinity of the CQDs (Muhammad Mailafiya et al. 2019; Zhou et al. 2017).

The CQDs were subjected to XRD scanning from 0° to 100° at room temperature, using a scanning rate of 2.00 (°/min). The resulting XRD data, as shown in SI 2, were analyzed to ascertain the crystallinity, nature, and phase purity of the CQDs. Notably, the CQDs exhibited distinct absorption peaks at 32.4° and 46.12° when measured at two theta angles within the range of 32° to 47°. Comparing values of the crystal lattice planes obtained from Bragg's law or equation for each nanomaterial with known crystal lattice planes for various materials, the lattice plane of graphene was closer to those obtained in our calculations. Graphene is a two-dimensional carbon allotrope composed of a single layer of carbon atoms arranged in a hexagonal lattice. Its lattice constant (the distance between adjacent carbon atoms) is approximately 0.246 nm, corresponding to 1.3932 Angstroms, which agrees that GQDs and CQDs are nanoparticles belonging to the same class and family (Yang et al. 2018).

While some less crystalline, less pure, and amorphous nanoparticles show broad absorption peaks, pure and crystalline nanoparticles exhibit narrower absorption peaks. The CQDs in this research show such narrow peaks, which indicates the presence of highly crystalline CQDs in our samples (Muhammad Mailafiya et al. 2019).

The efficiency of quenching in the CQDs-P_A system by AuNPs-P_T relies on the molar ratio (CQDs-P_A/AuNPs-P_T) (Sabzehparvar et al. 2019). To determine the FRET and quenching efficiency, we examined the fluorescence intensity of various proportions of these nanoconjugates and plotted the percentage FRET efficiency (E) against the ratios. The percentage FRET efficiency can be calculated using the following equation:

$$E = 1 - (F / F_0) \times 100$$

In this equation, E represents the amount of energy absorbed by the acceptor from the fluorophore divided by the amount absorbed by the donor fluorophore from the excitation source. F and F_0 denote the integrated fluorescence intensity of the donor in the presence and absence of the acceptor, respectively (Sabzehparvar et al. 2019; Shojaei et al. 2016).

By using different ratios of the prepared probe solution containing CQDs-P_A: AuNPs-P_T, ranging from 1:0, 1:1, 1:1.5, 1:2.3, 1:4, 1:9, to 1:19 (v/v), as the volume of AuNPs-P_T increases, the fluorescence intensity of CQDs-P_A diminishes, and the percentage increase in FRET efficiency or the quenching effect of AuNPs on CQDs-P_A with increasing volumes of the quencher (AuNPs-P_T). This quenching effect persists until the volume ratio reaches 1:9 (v/v), where it becomes evident that the fluorescence of the CQDs is almost entirely quenched (Shojaei et al. 2016).

However, this experiment aims to achieve a level of CQD fluorescence that enables fluorescence recovery upon adding analytes. Considering that the 1:1 (v/v) nanoconjugate resulted in a 76.2% suppression of the fluorescence intensity of CQDs-P_A, we selected a 1:1 (v/v) probe ratio for further applications. By combining a fixed volume of nanoconjugates (Probe) at the assumed ratio of 1:1 (v/v) with varying concentrations of cDNA

(ranging from 1×10^{-13} to 1×10^{-6} μM), we observed a turn-on fluorescence enhancement.

PERFORMANCE EVALUATION OF THE DEVELOPED BIOSENSOR

The biosensor system developed in this study exhibits remarkable performance, as demonstrated by the detection mechanism illustrated in Figure 1. The system comprises 9-mer sequences of amine-modified ssDNA probes attached to carbon quantum dots (CQDs), forming CQDs-P_A through amine coupling. Additionally, thiol-modified ssDNA probes with a length of 9-mer are attached to gold nanoparticles (AuNPs), resulting in AuNPs-PT through thiol coupling.

A synthetic complementary DNA (ctDNA) strand of the DEN-3 virus, consisting of 18 bases, is hybridized with the probes to detect the analyte. Each half of the ctDNA strand interacts with one of the 9-mer probes, forming a DNA duplex. This duplex formation induces steric hindrance between the nanoparticles, causing them to be positioned at a distance that enables fluorescence resonance energy transfer (FRET). The resulting fluorescence signal is directly proportional to the concentration of the analyte, ranging from 1×10^{-12} to 1×10^{-6} M (Figure 5). Notably, this phenomenon was not observed when non-complementary DNA (ncDNA) was used in place of the dengue sample. When distilled deionized water was used on the probe, the peak intensity was never increased with equal volume, and increasing the volume of the water decreased the peak intensity, due to the dilution effect. Therefore, we can conclude that the increase in fluorescence intensity corresponds to the concentration of the ctDNA (Nasrin et al. 2018; Sabzehparvar et al. 2019). The relationship between concentration and fluorescence enhancement efficiency falls within the linear concentration range of 0.001 nM to 100 nM, with a high correlation coefficient (R^2) of 0.979. This correlation is evident from the plot of fluorescence enhancement efficiency against concentration (Figure 5(c)).

To determine the limit of detection (LOD), a fundamental performance characteristic that represents the lowest concentration of an analyte reliably measurable by an analytical procedure (Shrivastava & Gupta 2011), we employed a method previously established in the literature (Noremylia et al. 2013). Applying this approach, we calculated the LOD for our biosensor to be 1.57 ± 0.71 nM, using the formula LOD = 3.3 Sb/SL. Here, Sb denotes the standard deviation of the response or the residual standard deviation of the linear regression line, and SL represents the slope of the regression line. The obtained LOD value of 1.57 ± 0.71 nM is consistent with the findings of other studies conducted by Gao et al. (2020), Sabzehparvar et al. (2019), Shamsipur et al. (2017), and Sun et al. (2014). Their reported LOD values ranged from 0.2 nM to 5.0 nM, as summarised in Table 2.

TABLE 2. Comparison of this' work LOD with previous reported value on fluorescence DNA based biosensors

Nanoparticle	Technique	Target Analytes	Linear Range	LOD	Ref
CDs/AuNPs	FRET	DNA-(PNA)	5 – 100 nM	0.21 nM	Gao et al. (2020)
CNBs	Fluorescence enhancement	HIV DNA	-	5.0 nM	Sun et al. (2014)
CdTe-QDs/ Cyanine5 (Cy5)	FRET	HPV18	1.0 – 50.0 nM	0.2 nM	Shamsipur et al. (2017)
CdSeTeS-QDs/ AuNPs	LSPR	Norovirus	10^{-14} – 10^{-9} g mL^{-1}	12.1×10^{-15} g mL^{-1}	Nasrin et al. (2018)
CdTe-QDs/AuNPs	RET	IBD virus	1×10^{-7} - 6×10^{-7} M	3.0 nM	Sabzehparvar et al. (2019)
CQDs/AuNPs	FRET	DENV	0.001 – 100 nM	1.5 nM	This work

Li = Naphthalimide, GO = Graphene oxide, CNBs = Carbon nanobelts, IBD virus = Infectious bursal disease virus, DENV = Dengue virus, LSPR = Localised Surface Plasmon Resonance, HPV18 = Human Papillomavirus 18 virus

The reproducibility study involved assessing the performance of the DNA biosensor (CQDs-NH-ssDNA and AuNPs-SH-ssDNA) across three sets of experiments, each using different concentrations of cDNA: 1000 nM, 100 nM, and 0.1 nM, respectively. In Table 3(a), five measurements of fluorescent intensity values were recorded for each concentration. Subsequently, these measurements were analyzed using the Stern-Volmer Equation to determine the interaction between the probe pair, resulting in fluorescence intensity recovery proportional to the cDNA concentration (Table 3(b)). By calculating the mean values, standard deviations (SD), and percentage relative standard deviations (%RSD), we obtained valuable insights into the reproducibility of the study. The consistent signals received from different measurements, as indicated by the measurement's percentage relative standard deviation (RSD), showed a constant reproducibility of the sensor signal. The relative standard deviations (RSD) of 4.5%, 2.7%, and 10% were achieved, showcasing the biosensor's high reliability of cDNA detection.

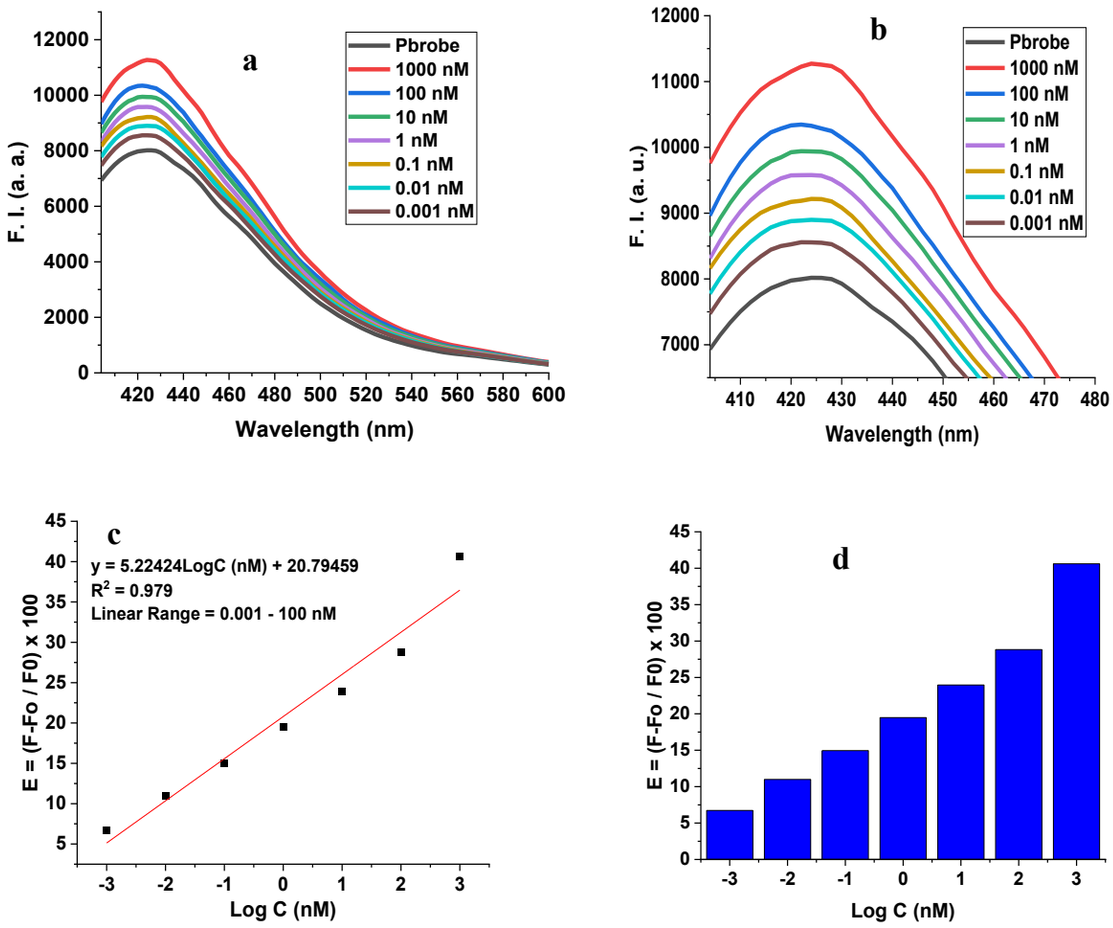

FIGURE 5. Result of detection of DEN-3 virus (a) Fluorescence enhancement signals of different concentrations of cDNA, (b) the magnified form of (a), (c) the calibration curve of the detection showing the fluorescence enhancement against the log C, (d) the bar chart representation of the calibration curve of the detection showing the fluorescence enhancement against the log C of mean results of (n = 3)

TABLE 3(a). Fluorescence intensity of selected analytes concentrations for reproducibility study

S/N0	Probe	1×10^{-6} M	1×10^{-7} M	1×10^{-10} M
1	7498	11439	10260	8920
2	7525	11545	10198	8948
3	8615	12810	11651	9938
4	8549	12789	11734	9930
5	8579	10960	10379	9504

TABLE 3(b). Statistical analysis of FRET efficiency of the responses of probes in Table 3(a) for reproducibility study of the probes

n	$E = (F- F_0 / F_0) \times 100$		
1	0.526	0.368	0.190
2	0.534	0.355	0.189
3	0.487	0.352	0.154
4	0.496	0.373	0.162
Mean	0.511	0.362	0.173
SD	0.023	0.010	0.019
%RSD	4.46	2.72	10.75

By calculating the mean values, standard deviations (SD), and percentage relative standard deviations (%RSD), we obtained valuable insights into the reproducibility of the study. The consistent signals received from different measurements, as indicated by the measurement's percentage relative standard deviation (RSD), showed a constant reproducibility of the sensor signal. The relative standard deviations (RSD) of 4.5%, 2.7%, and 10% were achieved, showcasing the biosensor's high reliability of cDNA detection.

To assess the selectivity and specificity of the FRET DNA biosensor platform, we conducted a comprehensive study comparing the reactions and tests of different types of DNA samples. Specifically, we examined the complementary DNA (cDNA), single-base mismatch DNA (1mDNA), and non-complementary DNA (ncDNA), all at a concentration of 1000 nM, using the developed probe system.

The critical distinction between ncDNA and cDNAlies in their inability to form a compatible sequence for conjugation. On the other hand, the 1mDNA differs from the probe by a single base pair, resulting in an incompatibility (Suria et al. 2020).

Figure 6(a) and 6(b) depicts the fluorescence recovery intensities observed for the cDNA, 1mDNA, and ncDNA. Notably, the cDNA exhibits the highest fluorescence intensity, followed by the 1mDNA and then the ncDNA. Conversely, the ncDNA demonstrates minimal intensity compared to the probe, as it fails to form a duplex and bring the fluorophore and acceptor

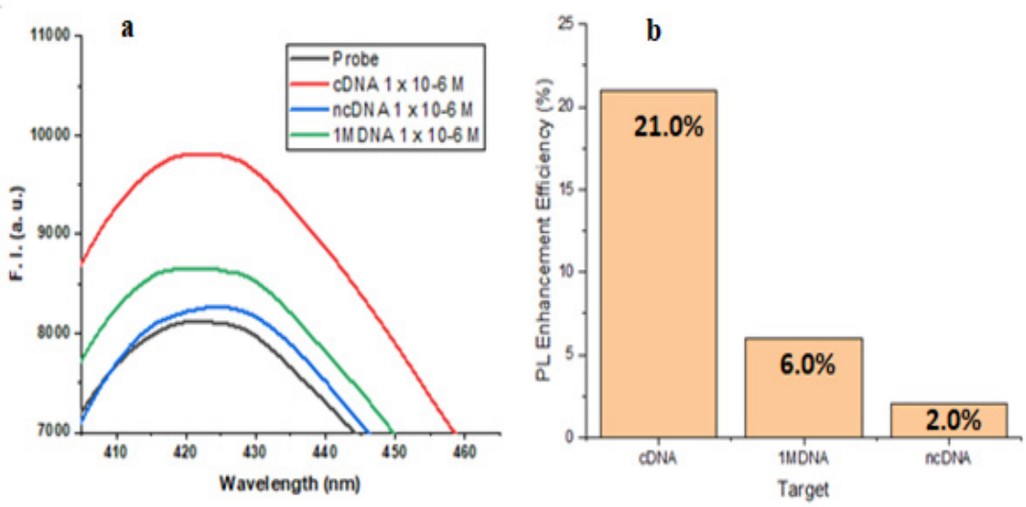

FIGURE 6. (a) Selectivity and specificity property of the probe with different targets, (b) % Recovery of the probe with the different conjugants (cDNA, 1MDNA, and ncDNA)

into proximity for FRET to occur. The slight increase in fluorescence intensity can be attributed to the irregular conjugation of complementary base pairs between the nucleic materials (probe and complementary analytes). This results in a marginal recovery in fluorescence intensity or a modest enhancement efficiency of only around 2%.

In contrast, the 1mDNA exhibits a fluorescence recovery of approximately 6%, surpassing the ncDNA. Remarkably, the cDNA showcases a fluorescence recovery of 21% compared to the ncDNA and the 1mDNA. This finding demonstrates that regardless of the DNA or RNA strands or sequences present in the matrix, the designed DNA biosensor exhibits selectivity and specificity towards the complementary sequence of DENV, enabling the formation of a duplex. Furthermore, the probe demonstrates robustness even in the presence of a single base pair difference between the cDNAand 1mDNA, as evidenced by the distinct disparity in fluorescence intensity.

Conclusions

In this study, CQDs were successfully synthesized from palm kernel shell biomass as a precursor and the synthesized CQDs and AuNPs were characterized using various instruments to study the chemical and morphological properties of the nanoparticles and nanoconjugates. The CQDs were utilized as fluorophores and electron donors in a FRET DNA biosensor system, while AuNPs are nano quenchers and electron acceptors. The process involved several steps: Firstly, the CQDs were functionalized with a carboxylic acid functional group and then modified with amine-modified ssDNA specific to the DEN-3 virus, an achievement obtained through an amine coupling reaction. Next, the AuNPs was synthesized and stabilized using RB which enhances their plasmon resonance properties and as well enhances dispersibility of the AuNPs in the solution and were functionalized with a carboxylic acid functional group using L-cysteine. Finally, using the thiol coupling technique, the nanoconjugate was modified with thiol-modified ssDNA specific to the DEN-3 virus.

The resulting nanoconjugate, formed by mixing the CQDs and AuNPs in a 1:1 ratio, exhibited a FRET phenomenon demonstrating high sensitivity and a low detection limit for synthetic complementary DEN-3 virus DNA strands. This biosensor design showed great promise in its sensitivity, selectivity, and specificity when tested with synthetic samples. It can potentially enable rapid and accurate detection of the DEN-3 virus within a linearity range of 0.001 nM to 100 nM. The sensitivity of the biosensor was calculated to be 5.22LogC + 20.79 (R = 0.979), and the limit of detection (LOD) for DENV-3 was determined to be 1.57 ± 0.71 nM.

ACKNOWLEDGMENTS

This work was supported by the Ministry of Science, Technology, and Innovation (MOSTI) Malaysia under MOSTI/RAN/DANA/RND(S)/1-8(19)(10).

REFERENCES

Adegoke, O. & Park, E.Y. 2017. Bright luminescent optically engineered core/alloyed shell quantum dots: An ultrasensitive signal transducer for dengue virus RNA via localized surface plasmon resonance-induced hairpin hybridization. *Journal of Materials Chemistry B* 5(16): 3047-3058. https://doi.org/10.1039/c7tb00388a

Bajpai, S.K., D'Souza, A. & Suhail, B. 2019. Blue light-emitting carbon dots (CDs) from a milk protein and their interaction with *Spinacia oleracea* leaf cells. *International Nano Letters* 9(3): 203-212. https://doi.org/10.1007/s40089-019-0271-9

Bhamore, J.R., Jha, S., Singhal, R.K., Park, T.J. & Kailasa, S.K. 2018a. Facile green synthesis of carbon dots from *Pyrus pyrifolia* fruit for assaying of Al^{3+} ion *via* chelation enhanced fluorescence mechanism. *Journal of Molecular Liquids* 264(2017): 9-16. https://doi.org/10.1016/j.molliq.2018.05.041

Bhamore, J.R., Jha, S., Park, T.J. & Kailasa, S.K. 2018b. Fluorescence sensing of Cu^{2+} ion and imaging of fungal cell by ultra-small fluorescent carbon dots derived from *Acacia concinna* seeds. *Sensors and Actuators, B: Chemical* 277: 47-54. https://doi.org/10.1016/j.snb.2018.08.149

Bhattacharya, D., Mishra, M.K. & De, G. 2017. Carbon dots from a single source exhibiting tunable luminescent colors through the modification of surface functional groups in ORMOSIL films. *Journal of Physical Chemistry C* 121(50): 28106-28116. https://doi.org/10.1021/acs.jpcc.7b08039

Chowdhury, A.D., Takemura, K., Khorish, I.M., Nasrin, F., Tun, M.M.N., Morita, K. & Park, E.Y. 2020. The detection and identification of dengue virus serotypes with quantum dot and AuNP regulated localized surface plasmon resonance. *Nanoscale Advances* 2(2): 699-709. https://doi.org/10.1039/c9na00763f

Darwish, N.T., Yatimah, B.A. & Khor, S.M. 2015. An introduction to dengue-disease diagnostics. *Trends in Analytical Chemistry* 67: 45-55. https://doi.org/10.1016/j.trac.2015.01.005

De, B. & Karak, N. 2013. A green and facile approach for the synthesis of water soluble fluorescent carbon dots from banana juice. *RSC Advances* 3(22): 8286-8290. https://doi.org/10.1039/c3ra00088e

Dong, W., Zhou, S., Dong, Y., Wang, J., Ge, X. & Sui, L. 2015. The preparation of ethylenediamine-modified fluorescent carbon dots and their use in imaging of cells. *Luminescence* 30(6): 867-871. https://doi.org/10.1002/bio.2834

Draz, M.S. & Shafiee, H. 2018. Applications of gold nanoparticles in virus detection. *Theranostics* 8(7): 1985-2017. https://doi.org/10.7150/thno.23856

Du, F., Zhang, M., Li, X., Li, J., Jiang, X., Li, Z., Hua, Y., Shao, G., Jin, J., Shao, Q., Zhou, M. & Gong, A. 2014. Economical and green synthesis of bagasse-Derived fluorescent carbon dots for biomedical applications. *Nanotechnology* 25(31): 315702. https://doi.org/10.1088/0957-4484/25/31/315702

E. Alahi, M.E. & Mukhopadhyay, S.C. 2017. Detection methodologies for pathogen and toxins: A review. *Sensors (Switzerland)* 17(8): 1885. https://doi.org/10.3390/s17081885

Gao, T., Xing, S., Xu, M., Fu, P., Yao, J., Zhang, X., Zhao, Y. & Zhao, C. 2020. A peptide nucleic acid–Regulated fluorescence resonance energy transfer DNA assay based on the use of carbon dots and gold nanoparticles. *Microchimica Acta* 187(7): 375. https://doi.org/10.1007/s00604-020-04357-w

Gao, Y., Zhu, Z., Xi, X., Cao, T., Wen, W., Zhang, X. & Wang, S. 2019. An aptamer-based hook-effect-recognizable three-line lateral flow biosensor for rapid detection of thrombin. *Biosensors and Bioelectronics* 133: 177-182. https://doi.org/10.1016/j.bios.2019.03.036

Gedda, G., Lee, C.Y., Lin, Y.C. & Wu, H.F. 2016. Green synthesis of carbon dots from prawn shells for highly selective and sensitive detection of copper ions. *Sensors and Actuators, B: Chemical* 224: 396-403. https://doi.org/10.1016/j.snb.2015.09.065

Gosink, J. 2014. Early laboratory diagnosis of dengue infections. *Medlab Magazine* 3: 014-016.

Guerrini, L., Alvarez-Puebla, R.A. & Pazos-Perez, N. 2018. Surface modifications of nanoparticles for stability in biological fluids. *Materials (Basel)* 11(7): 1154. https://doi.org/10.3390/ma11071154

Hamd-Ghadareh, S. & Salimi, A. 2019. DNA-functionalized dye-loaded carbon dots: Ultrabright FRET platform for ratiometric detection of Hg(II) in serum samples and cell microenvironment. *Ionics* 25(9): 4469-4479. https://doi.org/10.1007/s11581-019-02999-2

Hoan, B.T., Tam, P.D. & Pham, V-H. 2019. Green synthesis of highly luminescent carbon quantum dots from lemon juice. *Journal of Nanotechnology* 2019: 2852816. https://doi.org/10.1155/2019/2852816

Jahwarhar Izuan Abdul Rashid & Nor Azah Yusof. 2018. Laboratory diagnosis and potential application of nucleic acid biosensor approach for early detection of dengue virus infections. *Biosciences, Biotechnology Research Asia* 15(2): 245-255. https://doi.org/10.13005/bbra/2628

Laverdant, J., de Marcillac, W.D., Barthou, C., Chinh, V.D., Schwob, C., Coolen, L., Benalloul, P., Nga, P.T. & Maitre, A. 2011. Experimental determination of the fluorescence quantum yield of semiconductor nanocrystals. *Materials* 4(7): 1182-1193. https://doi.org/10.3390/ma4071182

Li, L., Li, L., Chen, C.P. & Cui, F. 2017. Green synthesis of nitrogen-doped carbon dots from ginkgo fruits and the application in cell imaging. *Inorganic Chemistry Communications* 86: 227-231. https://doi.org/10.1016/j.inoche.2017.10.006

Ma, X., Li, S., Hessel, V., Lin, L., Meskers, S. & Gallucci, F. 2019. Synthesis of luminescent carbon quantum dots by microplasma process. *Chemical Engineering and Processing - Process Intensification* 140: 29-35. https://doi.org/10.1016/j.cep.2019.04.017

Muhammad Mailafiya, M., Abubakar, K., Danmaigoro, A., Chiroma, S.M., Abdul Rahim, E.B., Mohd Moklas, M.A. & Zakaria, Z.A.B. 2019. Evaluation of *in vitro* release kinetics and mechanisms of curcumin-loaded cockle shell-derived calcium carbonate nanoparticles. *Biomedical Research and Therapy* 6(12): 3518-3540. https://doi.org/10.15419/bmrat.v6i12.580

Nasrin, F., Chowdhury, A.D., Takemura, K., Lee, J., Adegoke, O., Deo, V.K., Abe, F., Suzuki, T. & Park, E.Y. 2018. Single-step detection of norovirus tuning localized surface plasmon resonance-induced optical signal between gold nanoparticles and quantum dots. *Biosensors and Bioelectronics* 122: 16-24. https://doi.org/10.1016/j.bios.2018.09.024

Noremylia Mohd Bakhori, Nor Azah Yusof, Abdul Halim Abdullah & Mohd Zobir Hussein. 2013. Development of a fluorescence resonance energy transfer (FRET)-Based DNA biosensor for detection of synthetic oligonucleotide of *Ganoderma boninense*. *Biosensors* 3(4): 419-428. https://doi.org/10.3390/bios3040419

Nur Alia Sheh Omar, Yap Wing Fen, Jaafar Abdullah, Yasmin Mustapha Kamil, Wan Mohd Ebtisyam Mustaqim Mohd Daniyal, Amir Reza Sadrolhosseini & Mohd Adzir Mahdi. 2020. Sensitive detection of dengue virus Type 2 E-proteins signals using self-assembled monolayers/reduced graphene oxide-PAMAM dendrimer thin film-SPR optical sensor. *Scientific Reports* 10(1): 1-15. https://doi.org/10.1038/s41598-020-59388-3

Nur Alia Sheh Omar, Yap Wing Fen, Jaafar Abdullah, Che Engku Noramalina Che Engku Chik & Mohd Adzir Mahdi. 2018. Development of an optical sensor based on surface plasmon resonance phenomenon for diagnosis of dengue virus E-protein. *Sensing and Bio-Sensing Research* 20: 16-21. https://doi.org/10.1016/j.sbsr.2018.06.001

Plennevaux, E., Sabchareon, A., Limkittikul, K., Chanthavanich, P., Sirivichayakul, C., Moureau, A., Boaz, M., Wartel, T.A., Saville, M. & Bouckenooghe, A. 2016. Detection of dengue cases by serological testing in a dengue vaccine efficacy trial: Utility for efficacy evaluation and impact of future vaccine introduction. *Vaccine* 34(24): 2707-2712. https://doi.org/10.1016/j.vaccine.2016.04.028

Pudza, M.Y., Abidin, Z.Z., Abdul-Rashid, S., Md Yassin, F., Noor, A.S.M. & Abdullah, M. 2019. Synthesis and characterization of fluorescent carbon dots from tapioca. *ChemistrySelect* 4(14): 4140-4146. https://doi.org/10.1002/slct.201900836

Rashid, J.I.A., Yusof, N.A., Abdullah, J., Hashim, U. & Hajian, R. 2015. A novel disposable biosensor based on SiNWs/AuNPs modified-screen printed electrode for dengue virus DNA oligomer detection. *IEEE Sensors Journal* 15(8): 4420-4421. https://doi.org/10.1109/JSEN.2015.2417911

Sabzehparvar, F., Cherati, T.R., Mohsenifar, A., Shojaei, T.R. & Tabatabaei, M. 2019. Immobilization of gold nanoparticles with rhodamine to enhance the fluorescence resonance energy transfer between quantum dots and rhodamine; New method for downstream sensing of infectious bursal disease virus. *Spectrochimica Acta - Part A: Molecular and Biomolecular Spectroscopy* 212: 173-179. https://doi.org/10.1016/j.saa.2018.12.050

Saheeda, P., Sabira, K., Joseph, J. & Jayaleksmi, S. 2019. On the intriguing emission characteristics of size tunable carbon dots derived from functionalized multi-walled carbon nanotubes. *Materials Chemistry and Physics* 225: 8-15. https://doi.org/10.1016/j.matchemphys.2018.11.062

Samsulida Abdul Rahman, Rafidah Saadun, Nur Ellina Azmi, Nurhayati Ariffin, Jaafar Abdullah, Nor Azah Yusof, Hamidah Sidek & Reza Hajian. 2014. Label-free dengue detection utilizing PNA/DNA hybridization based on the aggregation process of unmodified gold nanoparticles. *Journal of Nanomaterials* 2014: 839286. https://doi.org/10.1155/2014/839286

Segal, L. & Eggerton, F.V. 1961. Infrared spectra of ethylenediamine and the dimethylethylenediamines. *Applied Spectroscopy* 15(4): 116-117. https://doi.org/10.1366/000370261774426939

Sentürk, E., Aktop, S., Sanlibaba, P. & Tezel, B.U. 2018. Biosensors: A novel approach to detect food-borne pathogens. *Applied Microbiology: Open Access* 4(3): 4-11. https://doi.org/10.4172/2471-9315.1000151

Shamsipur, M., Nasirian, V., Mansouri, K., Barati, A., Veisi-Raygani, A. & Kashanian, S. 2017. A highly sensitive quantum dots-DNA nanobiosensor based on fluorescence resonance energy transfer for rapid detection of nanomolar amounts of human papillomavirus 18. *Journal of Pharmaceutical and Biomedical Analysis* 136: 140-147. https://doi.org/10.1016/j.jpba.2017.01.002

Shojaei, T.R., Mohd Salleh, M.A., Sijam, K., Abdul Rahim, R., Mohsenifar, A., Safarnejad, R. & Tabatabaei, M. 2016. Detection of citrus tristeza virus by using fluorescence resonance energy transfer-based biosensor. *Spectrochimica Acta - Part A: Molecular and Biomolecular Spectroscopy* 169: 216-222. https://doi.org/10.1016/j.saa.2016.06.052

Shrivastava, A. & Gupta, V.B. 2011. Methods for the determination of limit of detection and limit of quantitation of the analytical methods. *Chronicles of Young Scientists* 2(1): 21-25. https://doi.org/10.4103/2229-5186.79345

Shylesh, Sankaranarayanapillai, Alex Wagener, Andreas Seifert, Stefan Ernst, and Werner R Thiel. 2010. Mesoporous organosilicas with acidic frameworks and basic sites in the pores: An approach to cooperative catalytic reactions. *Angewandte Chemie (International Edition)* 49(1): 184-187. https://doi.org/10.1002/anie.200903985

Stefanakis, D., Philippidis, A., Sygellou, L., Filippidis, G., Ghanotakis, D. & Anglos, D. 2014. Synthesis of fluorescent carbon dots by a microwave heating process: Structural characterization and cell imaging applications. *Journal of Nanoparticle Research* 16(10): Article No. 2646. https://doi.org/10.1007/s11051-014-2646-1

Sun, L-H., Wang, S., Shi, W-L., Zhang, S., Chen, X. & Cai, Q. 2012. A new type of anionic surfactant with four carboxylates for the preparation of mesoporous materials. *Frontiers of Materials Science* 6(3): 268-277. https://doi.org/10.1007/s11706-012-0173-5

Sun, X., Xing, Z., Ning, R., Asiri, A.M. & Obaid, A.Y. 2014. Carbon nanobelts as a novel sensing platform for fluorescence-enhanced DNA detection. *Analyst* 139(10): 2318-2321. https://doi.org/10.1039/c3an02364h

Suria Mohd Saad, Jaafar Abdullah, Suraya Abd Rashid, Yap Wing Fen, Faridah Salam & Lau Han Yih. 2020. A carbon dots based fluorescence sensing for the determination of *Escherichia coli* O157:H7. *Measurement: Journal of the International Measurement Confederation* 160: 107845. https://doi.org/10.1016/j.measurement.2020.107845

Tseng, M-H., Hu, C-C. & Chiu, T-C. 2019. A fluorescence turn-on probe for sensing thiodicarb using rhodamine b functionalized gold nanoparticles. *Dyes and Pigments* 171: 107674. https://doi.org/10.1016/j.dyepig.2019.107674

Wang, J. & Qiu, J. 2016. A review of carbon dots in biological applications. *Journal of Materials Science* 51(10): 4728-4738. https://doi.org/10.1007/s10853-016-9797-7

Wang, J., Zhang, P., Huang, C., Liu, G., Leung, K.C.F. & Wáng, Y.X.J. 2015. High performance photoluminescent carbon dots for *in vitro* and *in vivo* bioimaging: Effect of nitrogen doping ratios. *Langmuir* 31(29): 8063-8073. https://doi.org/10.1021/acs.langmuir.5b01875

Wasik, D., Mulchandani, A. & Yates, M.V. 2018. Salivary detection of dengue virus NS1 protein with a label-free immunosensor for early dengue diagnosis. *Sensors (Switzerland)* 18(8): 1-10. https://doi.org/10.3390/s18082645

WHO. 2018. Dengue Vaccines: WHO Position September 2018. *Weekly Epidemiological Record* 93 (36): 457-476. https://www.who.int/immunization/policy/position_papers/who_pp_dengue_2018_summary.pdf?ua=1

Wu, P., Li, W., Wu, Q., Liu, Y. & Liu, S. 2017. Hydrothermal synthesis of nitrogen-doped carbon quantum dots from microcrystalline cellulose for the detection of Fe^{3+} ions in an acidic environment. *RSC Advances* 7(70): 44144-44153. https://doi.org/10.1039/c7ra08400e

Xiao, Q., Chen, M., Nie, W., Xie, F., Yu, X. & Ma, C. 2023. A fluorescent biosensor for streptavidin detection based on double-hairpin DNA-templated copper nanoparticles. *Biosensors* 13(2): 168. https://doi.org/10.3390/bios13020168

Yakubu, N.M., Abdullah, J., Yusof, N.A., Abdul Rashid, S. & Shueb, R.H. 2021. Facile hydrothermal and solvothermal synthesis and characterization of nitrogen-doped carbon dots from palm kernel shell precursor. *Applied Science* 11(4): 1630. https://doi.org/https://doi.org/10.3390/app11041630

Yan, B., Wang, F., He, S., Liu, W., Zhang, C., Chen, C. & Lu, Y. 2022. Peroxidase-like activity of Ru–N–C nanozymes in colorimetric assay of acetylcholinesterase activity. *Analytica Chimica Acta* 1191: 339362. https://doi.org/10.1016/j.aca.2021.339362

Yang, G., Li, L., Lee, W.B. & Ng, M.C. 2018. Structure of graphene and its disorders: A review. *Science and Technology of Advanced Materials* 19(1): 613-648. https://doi.org/10.1080/14686996.2018.1494493

Yang, R., Guo, X., Jia, L., Zhang, Y., Zhao, Z. & Lonshakov, F. 2017. Green preparation of carbon dots with mangosteen pulp for the selective detection of Fe^{3+} ions and cell imaging. *Applied Surface Science* 423: 426-432. https://doi.org/10.1016/j.apsusc.2017.05.252

Yang, Z-C., Wang, M., Yong, A.M., Wong, S.Y., Zhang, X-H., Tan, H., Chang, A.Y., Li, X. & Wang, J. 2011. Intrinsically fluorescent carbon dots with tunable emission derived from hydrothermal treatment of glucose in the presence of monopotassium phosphate. *Chemical Communications* 47(42): 11615-11617.

Yin, B., Deng, J., Peng, X., Long, Q., Zhao, J., Lu, Q., Chen, Q., Li, H., Tang, H., Zhang, Y. & Yao, S. 2013. Green synthesis of carbon dots with down- and up-conversion fluorescent properties for sensitive detection of hypochlorite with a dual-readout assay. *Analyst* 138(21): 6551-6557. https://doi.org/10.1039/c3an01003a

Zhou, Y., Desserre, A., Sharma, S.K., Li, S., Marksberry, M.H., Chusuei, C.C., Blackwelder, P.L. & Leblanc, R.M. 2017. Gel-like carbon dots: Characterization and their potential applications. *ChemPhysChem* 18(8): 890-897. https://doi.org/10.1002/cphc.201700038

Zhang, G. 2013. Functional gold nanoparticles for sensing applications. *Nanotechnology Reviews* 2(3): 269-288. https://doi.org/10.1515/ntrev-2012-0088

*Corresponding author; email: jafar@upm.edu.my